Monthly Notices of the ROYAL ASTRONOMICAL SOCIETY

MNRAS **520,** 1997–2008 (2023) https://doi.org/10.1093/mnras/stad111
Advance Access publication 2023 January 11

ExoMol line lists – XLVIII. High-temperature line list of thioformaldehyde (H_2CS)

Thomas Mellor, Alec Owens, Jonathan Tennyson ★ and Sergei N. Yurchenko

Department of Physics and Astronomy, University College London, Gower Street, London WC1E 6BT, UK

Accepted 2023 January 3. Received 2022 December 28; in original form 2022 October 30

ABSTRACT

A comprehensive rotation–vibration (ro–vibrational) line list of thioformaldehyde ($^1H_2{}^{12}C^{32}S$) that is applicable for elevated temperatures (2000 K) is presented. The new MOTY line list covers the 0–8000 cm^{-1} range (wavelengths $\lambda > 1.3$ μm) and contains around 43.5 billion transitions between 52.3 million states with rotational excitation up to $J = 120$. Line list calculations utilize a newly determined empirically refined potential energy surface (PES) – the most accurate H_2CS PES to date – a previously published high-level *ab initio* dipole moment surface, and the use of an exact kinetic energy operator for solving the ro–vibrational Schrödinger equation. Post-processing of the MOTY line list is performed by replacing calculated energy levels with empirically derived values, vastly improving the accuracy of predicted line positions in certain spectral windows and making the line list suitable for high-resolution applications. The MOTY line list is available from the ExoMol data base at www.exomol.com and the CDS astronomical data base.

Key words: molecular data – opacity – planets and satellites: atmospheres – stars: atmospheres – ISM: molecules.

1 INTRODUCTION

Since its original interstellar detection (Sinclair et al. 1973), thioformaldehyde (main isotopologue $^1H_2{}^{12}C^{32}S$, henceforth referred to as H_2CS) has been observed in a variety of astronomical environments. For example, in massive star-forming regions such as Sagittarius B2 (Gardner, Whiteoak & Höglund 1980), where it can be efficiently formed through bimolecular reactions (Doddipatla et al. 2020), in galaxies which are nearby (Heikkilä, Johansson & Olofsson 1999; Martín et al. 2005) and more distant (Muller et al. 2011), molecular clouds (Esplugues et al. 2022), and in the comet Hale–Bopp (Woodney et al. 1997), which was the first detection of thioformaldehyde in a comet. Given that it is a simple organosulphur molecule, thioformaldehyde can be expected in the atmospheres of exoplanets, where sulphur chemistry is known to play a significant role in atmospheric composition (He et al. 2020; Hobbs et al. 2021). The need for accurate and complete molecular opacity data of H_2CS is a major driving force behind this work and the production of a new hot line list for the ExoMol data base (Tennyson et al. 2020).

Of interest here is the infrared (IR) rotation–vibration (ro–vibrational) spectrum of H_2CS, which has been the subject of numerous computational and experimental studies. Very recently, we performed a comprehensive analysis of the published experimental spectroscopic literature of H_2CS (Mellor et al. 2023) and extracted all meaningful transition data from 11 literature sources (Johnson & Powell 1970; Johns & Olson 1971; Beers et al. 1972; Fabricant, Krieger & Muenter 1977; Bedwell & Duxbury 1980; Turner, Halonen & Mills 1981; Mcnaughton & Bruget 1993; Clouthier et al. 1994; Flaud et al. 2008; Maeda et al. 2008; Müller et al. 2019). These data covered the ν_1, ν_2, ν_3, ν_4, ν_5, ν_6, and $2\nu_2$ vibrational bands of H_2CS and included transitions with rotational excitation up to $J = 54$, where J is the total angular momentum quantum number. Using the robust MARVEL (Measured Active Rotational−Vibrational Energy Levels) procedure (Császár et al. 2007; Furtenbacher, Császár & Tennyson 2007; Furtenbacher & Császár 2012; Tóbiás et al. 2019), we were able to validate 11 638 transitions to produce a highly accurate set of 4254 ro–vibrational energy levels, all labelled with unique quantum numbers and uncertainties. Such a data set of energy levels has been instrumental in producing a new line list of thioformaldehyde that is suitable for studying exoplanet atmospheres at high spectral resolution, where there are considerable demands on the accuracy of the line positions (Snellen 2014; Birkby 2018).

A previous room temperature line list of H_2CS was generated by Yachmenev, Polyak & Thiel (2013) and the computations utilized a highly accurate potential energy surface (PES) and dipole moment surface (DMS) constructed using state-of-the-art *ab initio* theory (Yachmenev et al. 2011). Just under 548 million transitions for ro–vibrational states up to $J = 30$ with band origins below 5000 cm^{-1} were computed using the variational nuclear motion code TROVE (Yurchenko, Thiel & Jensen 2007). Because the PES utilized was essentially *ab initio*, the accuracy of the predicted fundamental wavenumbers was limited to around 1−2 cm^{-1}, which is not sufficient for spectroscopic applications. To substantially improve the accuracy of the computed line positions, it is necessary to refine the PES to a set of empirical-quality energy levels such as the MARVEL H_2CS data set (Mellor et al. 2023) discussed above. Doing so can lead to orders-of-magnitude improvements in the accuracy of the transition wavenumbers and this procedure has been undertaken for this work. It is not necessary to perform any kind of

★ E-mail: j.tennyson@ucl.ac.uk

refinement to high-quality *ab initio* DMSs such as the H_2CS DMS of Yachmenev et al. (2013). Experience has shown that transition intensities computed using *ab initio* DMSs are often comparable to, and occasionally more reliable than experiment (Tennyson 2014; Yurchenko 2014; Bielska et al. 2022).

In this work, we present a newly computed comprehensive line list for H_2CS, named MOTY, that is suitable for elevated temperatures up to $T = 2000$ K. Although, using a very similar computational set-up to the room temperature line list calculations of Yachmenev et al. (2013), we have made two major developments to improve the accuracy and spectroscopic coverage of the new MOTY line list. The most significant improvement is the use of an empirically refined PES, the details of which are discussed in Section 2.3. Secondly, our variational ro–vibrational calculations of H_2CS employed an exact kinetic energy operator (KEO), which considerably improves convergence making the computations more tractable, thus allowing for greater energy level coverage and improved accuracy. The use of an exact KEO is the first application of its kind in TROVE to a polyatomic molecule and the details are reported in Section 2.1. Tailoring the MOTY line list towards high-resolution applications is detailed in Section 4.1, where we follow the ExoMolHD strategy (Yurchenko & Tennyson 2021) by replacing calculated energy levels with the empirically derived MARVEL values if available. Results and simulated spectra are presented in Section 5 and we conclude in Section 6.

2 VARIATIONAL NUCLEAR MOTION CALCULATIONS

Variational calculations used the nuclear motion programme TROVE, whose general methodology is well documented (Yurchenko et al. 2007, 2009; Yachmenev & Yurchenko 2015; Tennyson & Yurchenko 2017; Yurchenko, Yachmenev & Ovsyannikov 2017). TROVE calculations on H_2CS have been carried out previously when generating a room temperature line list (Yachmenev et al. 2013) and for validating a high-level *ab initio* PES of H_2CS (Yachmenev et al. 2011). We therefore summarize only the key steps in the calculation process and expand on the aspects that are novel to this work, namely the empirically refined PES and the use of an exact KEO. Generally speaking, ro–vibrational calculations were performed in the range $J = 0-120$ for each of the four irreducible representations A_1, A_2, B_1, and B_2 of the $\mathcal{C}_{2v}$(M) molecular symmetry group (Bunker & Jensen 1998) to obtain ro–vibrational energies (as eigenvalues) and wavefunctions (as eigenfunctions) of H_2CS. The Hamiltonian and basis functions used to construct the eigenfunctions were expressed in terms of the valence coordinates: r_{CS} (the C–S bond), r_{CH_1}, and r_{CH_2} (the C–H bonds), α_{SCH1} and α_{SCH_2} (the H–C–S angles), and τ (the dihedral angle between the H–C–S planes). The DMS was also expressed in terms of these coordinates, and along with the eigenfunctions, was used to compute ro–vibrational line intensities using the GPU-code MPI-GAIN (Al-Refaie, Yurchenko & Tennyson 2017).

2.1 Kinetic energy operator

TROVE usually employs an approximate KEO that is constructed as a power series expansion in terms of linearized coordinates when solving the ro–vibrational Schrödinger equation. Here, an exact analytic expression in terms of the valence coordinates has been derived and implemented as an external input for the TROVE calculations. Benefits of using an exact KEO are more accurate results and a refined PES that can be used in other nuclear motion codes. Expressing the Hamiltonian in terms of valence coordinates should also be expected to result in faster convergence in the computed energy levels, especially at high J_s, reducing the computational burden and allowing for the use of a more compact ro–vibrational basis set (Yachmenev & Yurchenko 2015).

For the KEO, a (right-handed) body-fixed frame was chosen such that the x-axis bisected the dihedral angle τ, the z-axis pointed along the C–S bond, and the frame's origin was at the centre of mass of the nuclei. The KEO was represented in a sum-of-products form which enabled it to be used by the program TROVE with only minor modifications. In this representation, each G matrix element in the KEO operator (and the pseudo-potential part, see Yurchenko et al. 2007 for details) has the form

$$\sum_{ijklmn} a_{ijklmn} f^i_{CS}(r_{CS}) f^j_{CH_1}(r_{CH_1}) f^k_{CH_2}(r_{CH_2}) f^l_{SCH_1}(\alpha_{SCH_1}) \times f^m_{SCH_2}(\alpha_{SCH_2}) f^n_\tau(\tau), \quad (1)$$

where the a_{ijklmn} are the coefficients and the f_s label functions of the different coordinates. For each mode, there is a finite set of functions. For the bond lengths, they are

$$\frac{1}{r}, \frac{1}{r^2}, \frac{1}{r^3}, \frac{1}{r^4}. \quad (2)$$

For the bond angles, they are

$$\cos\alpha,\ \cot\alpha,\ \csc\alpha,\ \sin\alpha,\ \cot^2\alpha,\ \cot\alpha\csc\alpha,\ \csc^2\alpha. \quad (3)$$

Finally, for the dihedral angle, they are

$$\cos(\tau/2),\ \sin(\tau/2),\ \cos^2(\tau/2),\ \cos(\tau/2)\sin(\tau/2),\ \sin^2(\tau/2). \quad (4)$$

The KEO was constructed using the Sørensen (1979) method that assumes the so-called Wilson integration volume with a Jacobian equals to 1. The full KEO is reproduced in Appendix A.

2.2 Ro-vibrational basis set

TROVE uses a three-step construction process to build the symmetry-adapted ro–vibrational basis set. In step 1, one-dimensional primitive basis functions ϕ_{v_i}, where v_i corresponds to the ith function for the vth vibrational mode, are calculated numerically for each vibrational degrees of freedom (dof; six in total for H_2CS) by integrating the respective one-dimensional vibrational Schrödinger equations using the Numerov−Cooley method (Noumerov 1924; Cooley 1961). The one-dimensional Hamiltonian is generated by freezing all vibrational modes except the one of interest.

At step 2, the symmetry-adapted vibrational basis set ($J = 0$) is formed from four independent subsets of the Numerov–Cooley primitive basis functions ϕ_{v_i} for the (i) C–S stretch, (ii) C–H_1 and C–H_2 stretches, (iii) H_1–C–S and H_2–C–S bending modes, and (iv) τ dihedral out-of-plane mode by solving the corresponding reduced-mode vibrational Schrödinger equations. The reduced-mode Hamiltonian is formed by integrating out the modes for the other subsets using their ground Numerov–Cooley eigenfunctions. These reduced-mode eigenfunctions are symmetrized according to the irreducible representations of the molecular symmetry group $\mathcal{C}_{2v}$(M) and form the basis functions for solving the full six-dimensional $J = 0$ problem. For H_2CS, a vibrational basis set cut-off was applied based on a polyad number truncation scheme,

$$P = v_{CS} + 2(v_{CH_1} + v_{CH_2}) + v_{H_1CS} + v_{H_2CS} + v_\tau \le P_{max}, \quad (5)$$

which used the polyad cut-off $P_{max} = 14$, chosen to ensure that full ro–vibrational calculations were computationally tractable when

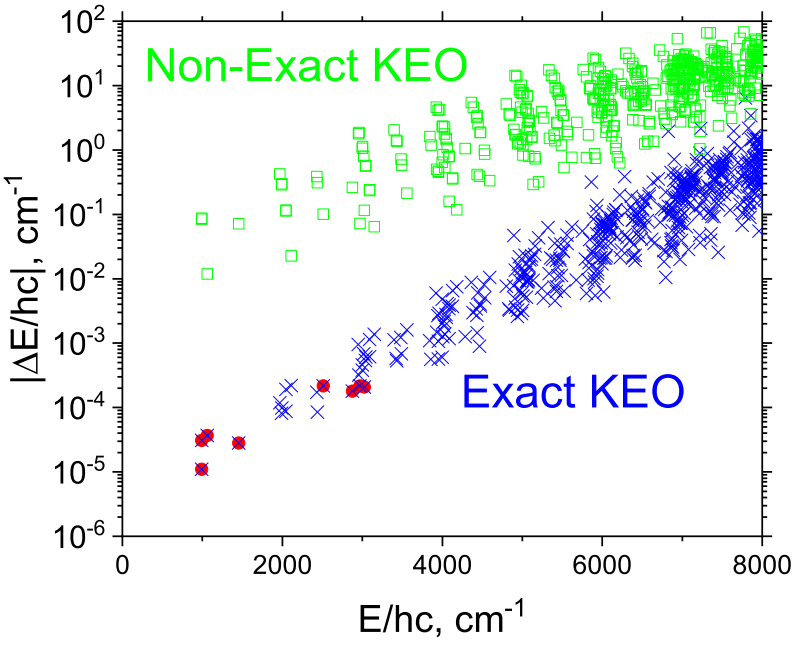

Figure 1. Convergence of the vibrational ($J = 0$) TROVE calculations as a difference between $P = 14$ and 16 energy term values H_2CS (cm^{-1}). The blue crosses correspond to the calculations using the new exact KEO implementation in TROVE; the green squares correspond to calculations using the approximate, linearized KEO version of TROVE as in Yachmenev et al. (2011, 2013). The red circles indicate states used in the refinement of the spectroscopic model.

generating a line list up to very high J (as discussed by Yachmenev et al. 2013).

The final ro–vibrational basis set for $J > 0$ computations is then formed as a contracted product of these vibrational functions $\Phi_{i_{\rm vib}}^{J=0,\Gamma_{\rm vib}}$ (7912 functions) and symmetrized rigid rotor wavefunctions $|J, K, \Gamma_{\rm rot}, m\rangle$ as given by

$$\Psi_{i_{\rm vib},K}^{J,\Gamma} = \left\{ \Phi_{i_{\rm vib}}^{J=0,\Gamma_{\rm vib}} \times |J, K, \Gamma_{\rm rot}, m\rangle \right\}^{\Gamma}, \tag{6}$$

where Γ, $\Gamma_{\rm vib}$, and $\Gamma_{\rm rot}$ are the total, vibrational, and rotational symmetries in $\mathcal{C}_{2v}$(M), $K = |k|$, k and m is the projection of the angular momentum on the molecular z and laboratory Z-axis, respectively, and $i_{\rm vib}$ is a TROVE vibrational index to count the $\Phi_{i_{\rm vib}}^{J=0,\Gamma_{\rm vib}}$ functions regardless of their symmetry. For further details of the TROVE symmetry adaptation and contraction procedure, see Yurchenko et al. (2017).

For H_2CS, the TROVE wavefunctions were assigned the following ro–vibrational quantum numbers: v_1, v_2, v_3, v_4, v_5, v_6, J, K, Γ, $\Gamma_{\rm vib}$, and $\Gamma_{\rm rot}$, which can be correlated to the spectroscopic (normal mode) quantum numbers commonly encountered. Details of the mapping between the two, which is essential for 'MARVELizing' the final MOTY line list, i.e. replacing the computed energy levels with the more accurate MARVEL values, will be discussed in Section 4.1.

In order to assess the convergence of the TROVE $P = 14$ vibrational basis set used in calculations, a larger basis set with $P = 16$ was used to compute the vibrational $J = 0$ energies of H_2CS using the same refined PES (see below). Fig. 1 shows the differences between the $P = 14$ and 16 term values. Below 6000 cm^{-1} the differences are within 0.1 cm^{-1}, which then gradually increase to up to 1 cm^{-1} below 8000 cm^{-1} with a few states reaching up to 10 cm^{-1}. This convergence should be better than the expected 'detuning' of the empirical PES, considering that the experimentally determined vibrational states do not extend beyond 3050 cm^{-1}, indicated in this figure by red circles.

In Fig. 1, we also demonstrate that the basis set convergence of the current ro–vibrational calculations based on the new implementations of the exact KEO of H_2CS in TROVE is a significant improvement compared to the TROVE calculation by Yachmenev et al. (2011, 2013), where an approximate, linearized Hamiltonian operator was used. Here, we show analogous energy differences between the $P = 14$ and 16 vibrational calculations of H_2CS using the approximate linearized TROVE model in conjunction with the refined PES from this work. The improvement in the basis set convergence of 2–3 orders of magnitude is due to the new KEO in TROVE.

2.3 Potential energy surface and empirical refinement

The PES used in this work is based on an *ab initio* surface originally generated by Yachmenev et al. (2011), which utilized state-of-the-art electronic structure methods in the calculation process. The PES was represented as an expansion in terms of six valence coordinates,

$$\xi_i = 1 - \exp[-b_i(r_i - r_i^{\rm e})], \quad i = {\rm CS}, {\rm CH}_1, {\rm CH}_2, \tag{7}$$

$$\xi_j = \alpha_j - \alpha_j^{\rm e}, \quad j = {\rm SCH}_1, {\rm SCH}_2, \tag{8}$$

$$\xi_6 = 1 + \cos\tau. \tag{9}$$

Here, $r_{\rm CS}$, $r_{\rm CH_1}$, and $r_{\rm CH_2}$ are the bond lengths, $\alpha_{\rm SCH_1}$ and $\alpha_{\rm SCH_2}$ are the bond angles, τ is the dihedral angle between the SCH_1 and SCH_2 planes, and b_i is a Morse oscillator parameter. The PES was expressed analytically as,

$$V = \sum_{ijklmn} a_{ijklmn} \xi_{\rm CS}^i \xi_{\rm CH_1}^j \xi_{\rm CH_2}^k \xi_{\rm SCH_1}^l \xi_{\rm SCH_2}^m \xi_\tau^n, \tag{10}$$

where a_{ijklmn} are the expansion parameters with maximum expansion order $i + j + k + l + m + n = 6$ with the linear expansion parameters fixed to zero. A total of 413 parameters were utilized including the three equilibrium ($r_{\rm CS}^{\rm e}$, $r_{\rm CH}^{\rm e}$, $\alpha_{\rm SCH}^{\rm e}$) and two Morse parameters ($b_{\rm CH}$, $b_{\rm CS}$). The expansion parameters assumed the values of the *ab*

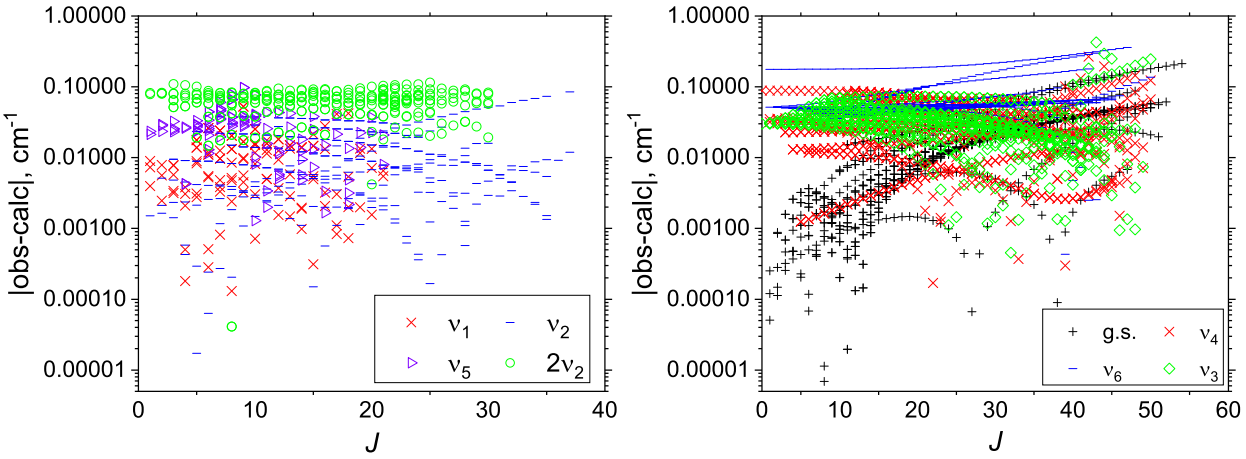

Figure 2. The fitting residual errors (O−C), i.e. the energy difference (in cm^{-1}) between the empirically derived MARVEL energies and computed TROVE values, as a function of the total angular momentum quantum number J. Residual errors are shown for seven vibrational bands and have been computed using the newly refined PES of H_2CS.

Table 1. Extract from a `.trans` file of the H_2CS MOTY line list.

f	i	A_{fi} (s^{-1})
1967530	2157952	5.6990e−01
9281842	9684141	2.1589e−11
21248596	21941059	2.5861e−12
5252014	5149230	9.6459e−04
12481388	12623346	8.6482e−11
1781054	1841556	2.4679e−16

Notes. f: upper state counting number; *i:* lower state counting number; A_{fi}: Einstein-A coefficient (in s^{-1}).

initio PES from Yachmenev et al. (2011), with only the quadratic expansion parameters (14 in total) varied in the refinement to the empirically derived MARVEL energy levels. The refinement used H_2CS MARVEL energies for $J = 0$, 1, 2, 3, 4, 5, 8, 10 (448 in total) covering the ground, ν_1, ν_2, ν_3, ν_4, ν_5, ν_6, and $2\nu_2$ vibrational bands. For the equilibrium structural parameters, we used the optimized geometry values from Yachmenev et al. (2013): $r^e_{CS} = 1.608\,952$ Å, $r^e_{CH} = 1.086\,848$ Å, and $\alpha^e_{SCH} = 121.750°$. To ensure the refined PES maintained a realistic shape and gave reliable results in regions not sampled by the MARVEL data, the PES was constrained to the *ab initio* PES of Yachmenev et al. (2011) in the fitting.

The refinement showed very quick convergence. The quality of the fit is demonstrated in Fig. 2, where we have plotted the fitting residuals, i.e. the energy difference (in cm^{-1}) between the MARVEL and computed TROVE H_2CS values, for the seven vibrational states used in the refinement. The majority of the fitting residuals are all below 0.1 cm^{-1}, see Fig. 2, notably for the ground state which is to be expected since it corresponds to the lowest part of the PES. The errors are substantially smaller than those of the original *ab initio* H_2CS PES of Yachmenev et al. (2011), which would be in the region of 1–5 cm^{-1}, demonstrating the improvements in accuracy that can be achieved with a refined PES. A FORTRAN version of the PES is given in the supporting information.

2.4 Dipole moment surfaces

A previously published *ab initio* DMS was utilized for intensity calculations. The DMS of Yachmenev et al. (2013) was computed using coupled cluster theory CCSD(T) in conjunction with the augmented correlation-consistent basis set aug-cc-pVQZ(+d for S) (Dunning Jr 1989; Dunning Jr, Peterson & Wilson 2001). This DMS has already been used in room temperature line list calculations of H_2CS and with the *ab initio* PES was able to accurately reproduce complicated resonance effects, such as intensity borrowing, when modelling several vibrational bands affected by strong Coriolis coupling. The three dipole components making up the DMS were represented analytically using a sum-of-products expansion in terms of linear expansion variables for the six vibrational coordinates (further details can be found in Yachmenev et al. 2013).

3 THE MOTY LINE LIST OF H_2CS

The newly computed line list for H_2CS, called MOTY, contains 43 56 116 660 transitions between 52 292 454 states and covers the 0–8000 cm^{-1} range for ro–vibrational states with rotational excitation up to $J = 120$. The lower and upper state energy thresholds were chosen to be 8000 and 18000 cm^{-1}, respectively. The MOTY line list is provided in the ExoMol data format (Tennyson, Hill & Yurchenko 2013) and an extract from one of the `.trans` transition files and from the `.states` states file is shown in Tables 1 and 2, respectively. The `.trans` files are divided into 1000 cm^{-1} wavenumber ranges to make them more manageable and they contain upper and lower state ID numbers along with the Einstein A coefficient (in s^{-1}) of the transition between the states. The `.states` file contains a list of the ro–vibrational states of H_2CS with state ID numbers, energies (in cm^{-1}), uncertainties (in cm^{-1}), state lifetimes, and unique quantum numbers. Both the standard spectroscopic normal mode quantum numbers and TROVE quantum numbers are included in the `.states` file and the mapping between the two sets is discussed in Section 4, with 'MARVELization' of the MOTY line list detailed in Section 4.1.

As is standard now for ExoMol line lists, all molecular states possess an uncertainty. The uncertainties were defined either as the MARVEL uncertainty if available, or estimated via the expression (in cm^{-1}):

$$\text{unc} = 0.4n_1 + 0.2(n_2 + n_3 + n_4 + n_5 + n_6) + 0.002J(J+1), \quad (11)$$

where n_1–n_6 are the TROVE quantum numbers. These uncertainties are only approximate and grow steadily with increasing rotational and vibrational excitation, where we tend to be conservative in estimating

Table 2. Extract from the `.states` file of the H_2CS MOTY line list.

i	$\tilde{E}$ (cm^{-1})	g	J	δ (cm^{-1})	τ (s^{-1})	$\Gamma_{\rm tot}$	v_1	v_2	v_3	v_4	v_5	v_6	$\Gamma_{\rm vib}$	J	K_a	K_c	i_v	$\lvert C_i^2\rvert$	n_1	n_2	n_3	n_4	n_5	n_6	Ca/Ma	$\tilde{E}_{\rm T}$ (cm^{-1})
1	0.000 000	1	0	0.000 001	Inf	A1	0	0	0	0	0	0	A1	0	0	0	1	1.0	0	0	0	0	0	0	Ma	0.000 000
2	1059.204 475	1	0	0.000 460	8.3703E−01	A1	0	0	1	0	0	0	A1	0	0	0	4	1.0	1	0	0	0	0	0	Ma	1059.234 861
3	1455.496 493	1	0	0.100 000	1.6832E+00	A1	0	1	0	0	0	0	A1	0	0	0	5	1.0	0	0	0	1	0	0	Ca	1455.496 493
4	1966.570 835	1	0	0.200 000	2.3271E−01	A1	0	0	0	0	0	2	A1	0	0	0	6	1.0	0	0	0	1	1	0	Ca	1966.570 835
5	1992.435 721	1	0	0.200 000	1.6450E−01	A1	0	0	0	2	0	0	A1	0	0	0	8	1.0	0	0	0	0	0	2	Ca	1992.435 721
6	2109.341 721	1	0	0.200 000	4.2379E−01	A1	0	0	2	0	0	0	A1	0	0	0	11	1.0	2	0	0	0	0	0	Ca	2109.341 721
7	2510.397 221	1	0	0.200 000	5.6662E−01	A1	0	1	1	0	0	0	A1	0	0	0	14	1.0	1	0	0	1	0	0	Ca	2510.397 221
8	2877.032 488	1	0	0.200 000	1.3711E−01	A1	0	2	0	0	0	0	A1	0	0	0	15	1.0	0	0	0	1	1	0	Ca	2877.032 488
9	2971.028 217	1	0	0.200 000	3.3900E−02	A1	1	0	0	0	0	0	A1	0	0	0	18	1.0	0	0	1	0	0	0	Ca	2971.028 217
10	3017.401 926	1	0	0.300 000	1.8251E−01	A1	0	0	1	0	0	2	A1	0	0	0	21	1.0	1	0	0	1	1	0	Ca	3017.401 926
11	3043.141 281	1	0	0.300 000	1.4094E−01	A1	0	0	1	2	0	0	A1	0	0	0	24	1.0	1	0	0	0	0	2	Ca	3043.141 281
12	3150.274 608	1	0	0.300 000	2.8533E−01	A1	0	0	3	0	0	0	A1	0	0	0	27	1.0	3	0	0	0	0	0	Ca	3150.274 608

Notes. i: state identifier; $\tilde{E}$: state term value; g: state degeneracy; J: state rotational quantum number; δ: energy uncertainty; τ: lifetime; $\Gamma_{\rm tot}$: total symmetry in C_{2v}(M); v_1–v_6: normal mode vibrational quantum numbers; $\Gamma_{\rm vib}$: symmetry of vibrational contribution in C_{2v}(M); J: state rotational quantum number; K_a and K_c: state oblate and prolate quantum numbers; i_v: vibrational state ID; $|C_i^2|$: largest coefficient used in the assignment; n_1–n_6: TROVE vibrational quantum numbers; Ca/Ma: Label indicating if the term value is based on the MARVEL (Ma) or the MOTY energy list (Ca); $\tilde{E}_{\rm AYTY}$: original MOTY state term value.

values for highly excited states. It is important for users of the MOTY line list to be aware that transitions that are suitable for high-resolution applications possess a defined (MARVEL) uncertainty, and those have uncertainties devined by equation (11) are not for high-resolution studies. States with an estimated uncertainty may well be highly accurate, however, without experimental verification this is difficult to verify.

The temperature-dependent partition function $Q(T)$ of H_2CS has been computed on a 1 K grid in the 1–2000 K range and is available as a `.pf` file from the ExoMol website. Partition function values were computed by summing over all the computed ro–vibrational states of the MOTY line list and used nuclear spin statistical weights of $g_{\rm ns} = 1, 1, 3, 3$ for states of symmetry A_1, A_2, B_1, and B_2, respectively. The dependence of $Q(T)$ on temperature is illustrated in Fig. 3, where we also show the partition function values from the Cologne Database for Molecular Spectroscopy (CDMS; Endres et al. 2016) data base. The latter only contains ground vibrational transitions which explains the lower value at $T = 500$ K.

As part of the ExoMol services, cross-sections of H_2CS are provided via the ExoMol cross-sections app. The app can be used, for example, to generate absorption cross-sections of H_2CS with the Doppler broadening line profile for temperatures from 100 to 2000 K covering the wavenumber range from 0 to 8000 cm^{-1} on a grid with a resolution of up to 0.01 cm^{-1} (Hill, Yurchenko & Tennyson 2013). We also provide the H_2CS spectroscopic model used in TROVE calculations in the form of a TROVE input file, containing the potential energy and DMS parameters as well as the basis set specifications. This input file can be used with the FORTRAN code TROVE freely available from GitHub via www.github.org/exomol.

4 MAPPING BETWEEN TROVE AND NORMAL MODE QUANTUM NUMBERS

To provide the line list with both the TROVE quantum numbers and the normal mode vibrational quantum numbers, a mapping between the two is necessary. The TROVE local mode quantum numbers v_i are related to the primitive basis functions ϕ_{v_i} that are used to build the full symmetry-adapted basis set in ro–vibrational calculations. Here, $v_{\rm CS}$, $v_{\rm CH_1}$, and $v_{\rm CH_2}$ correspond to the stretching dof, $v_{\rm H_1CS}$ and $v_{\rm H_2CS}$ to the bending dof, and v_τ to the dihedral angle. The TROVE local mode quantum numbers $v_i^{\rm Ca}$ are used to label the calculated ro–vibrational states based on the highest contribution from the different primitive basis functions. To be of use, they must be correlated to the standard spectroscopic normal mode quantum numbers n_i. The following relations between the normal mode n_i and TROVE local mode quantum numbers v_i apply:

$$\begin{aligned} n_1 &= v_2^{\rm Ca}, \\ n_2 + n_5 &= v_2^{\rm Ca} + v_3^{\rm Ca}, \\ n_3 + n_6 &= v_4^{\rm Ca} + v_5^{\rm Ca}, \\ n_4 &= v_6^{\rm Ca}; \end{aligned}$$

these are also detailed in Table 3, which shows the mapping between the local and normal modes for the vibrational modes in H_2CS.

To correlate the TROVE rotational quantum numbers J, K, and $\Gamma_{\rm rot}$ to the standard rotational quantum numbers for H_2CS J^{K_a,K_c}, we first note that the TROVE quantum number K coincides with K_a, while K_c is reconstructed using the standard spectroscopic rules as described by Bunker & Jensen (1998), see their table 12-9. The relationship between K_a and K_c with rotational symmetry is listed in Table 4.

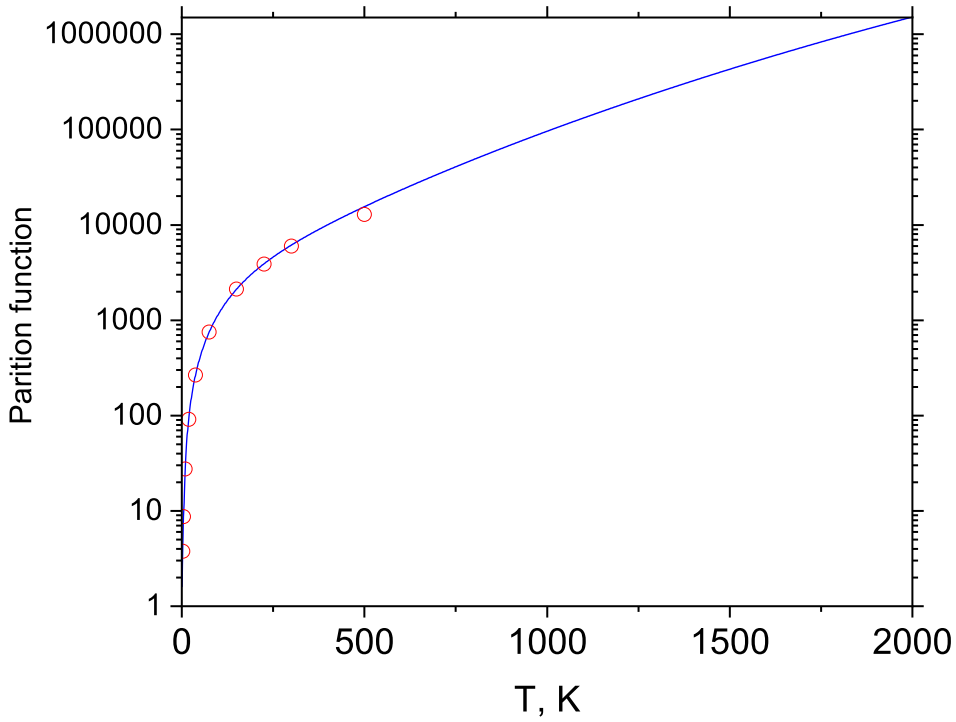

Figure 3. Temperature dependence of the partition function $Q(T)$ of H_2CS computed using the MOTY line list (solid line) and compared to the CDMS values (Endres et al. 2016; circles).

Table 3. Mapping between the TROVE local modes and the standard normal mode notation ν_i. Here, Γ is the symmetry of the fundamental mode in $\mathcal{C}_{2v}$(M).

Γ	Vibrations	Normal mode, ν	TROVE modes
A_1	C–H symm. stretch	ν_1	2 and 3
A_1	S–C–H symm. bend	ν_2	4 and 5
A_1	S–C stretch	ν_3	1
B_1	Out-of-plane	ν_4	6
B_2	C–H asymm. stretch	ν_5	2 and 3
B_2	S–C–H asymm. bend	ν_6	4 and 5

Table 4. Mapping between the rotational symmetry Γ_{rot} in $\mathcal{C}_{2v}$(M) and rotational quantum numbers K_a, K_c used for H_2CS (Bunker & Jensen 1998).

K_a, K_c	Γ_{rot}	K_a, K_c	Γ_{rot}
Even, even	A_1	Odd, even	B_2
Even, odd	A_2	Odd, odd	B_1

4.1 MARVELization of the line list

Following the ExoMolHD strategy (Yurchenko & Tennyson 2021), in order to improve the accuracy of the MOTY line list and tailor it to high-resolution applications, the calculated energy levels are replaced with the empirically derived MARVEL values, if available. To this end, the MARVEL and TROVE computed energies have to be matched by correlating their quantum numbers.

Table 5 lists the previously described correlation for the eight vibrational bands used in the MARVELization of the H_2CS line list. To be efficient, the correlation is built via the TROVE vibrational quantum index i_{vib} as indicated in Table 5, see also equation (6), where i_{vib} is used to identify the vibrational basis functions $\Phi_{i_{vib}}^{J=0,\Gamma_{vib}}$.

Table 5. Mapping between the TROVE local mode quantum numbers v_i and the standard normal mode notations $n\,\nu_i$ for the states used in the MARVELization. Here, Γ is the symmetry of the fundamental mode in $\mathcal{C}_{2v}$(M) and i_{vib} is a TROVE counting index identifying the vibrational ($J = 0$) states, see equation (6).

State	Γ	v_1	v_2	v_3	v_4	v_5	v_6	i_{vib}
g.s.	A_1	0	0	0	0	0	0	1
ν_4	B_1	0	0	0	0	0	1	2
ν_6	B_2	0	0	0	0	1	0	3
ν_3	A_1	1	0	0	0	0	0	4
ν_2	A_1	0	0	0	1	0	0	5
$2\nu_2$	A_1	0	0	0	1	1	0	15
ν_1	A_1	0	0	1	0	0	0	18
ν_5	B_2	0	1	0	0	0	0	22

5 SPECTRA SIMULATIONS

All spectra simulations used the open source program EXOCROSS (Yurchenko, Al-Refaie & Tennyson 2018; see github.com/exomol). In Fig. 4, a general overview of the H_2CS spectrum at three different temperatures (296, 1000, and 2000 K) is plotted. Absolute absorption cross-sections were computed at a resolution of 1 cm^{-1} using a Gaussian line profile with a half width at half-maximum (HWHM) of 1 cm^{-1}. As expected, the higher temperature spectra exhibit spectral flattening as the previously weaker features gain intensity.

A more detailed band-by-band illustration of the room temperature spectrum of H_2CS is shown in Fig. 5.

In Fig. 6 (left-hand panel), a comparison of a synthetic microwave spectrum of H_2CS between the MOTY ExoMol line list and the CDMS (Müller et al. 2001, 2005) is given. The good agreement of the intensities indicate that the equilibrium dipole moments used in CDMS and the MOTY line list agree well. The CDMS line list is

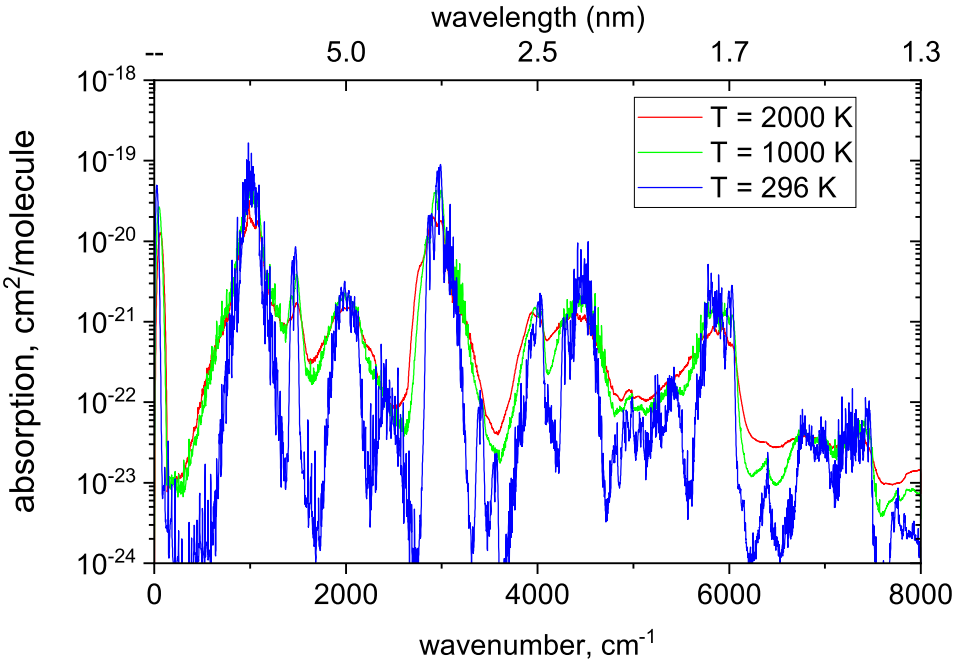

Figure 4. Absorption cross-sections of H_2CS at $T = 296$, 1000 , and 2000 K. A Gaussian line profile with a HWHM of 1 cm^{-1} was used on a grid of resolution 1 cm^{-1}.

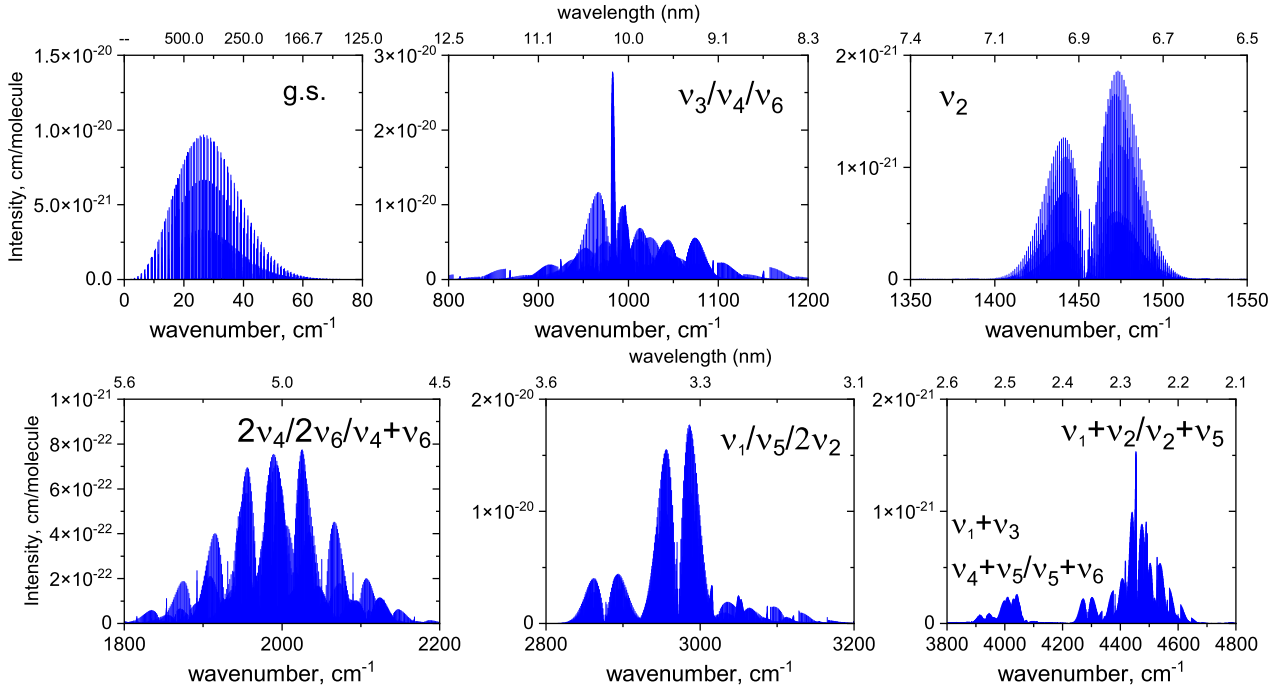

Figure 5. Overview of the strongest bands of H_2CS at $T = 296$ K.

based on a dipole moment value of 1.6491 D due to Fabricant et al. (1977). Our *ab initio* dipole moment gives an expectation value of 1.648 72 D for the ground vibrational state. These values can also be compared to an experimental laser-Stark value of 1.6483 D obtained by Cox, Hubbard & Kato (1982).

The right-hand panel of Fig. 6 shows a comparison with a high-resolution spectrum of H_2CS by Flaud et al. (2008) for the $\nu_3/\nu_4/\nu_6$ region, although the experimental data only give relative intensities. The agreement is excellent. Further confirmation of the reliability of the MOTY line list intensities can be seen when comparing to recent theoretical calculations by Erfort, Tschöpe & Rauhut (2020), which gave an intensity of 1.01×10^{-20} cm molecule^{-1} (Erfort et al. 2020; using coupled cluster theory, CCSD(T)/cc-pVTZ) for the ν_4 transition $3_{03} \leftarrow 3_{13}$, compared to our value of 1.02×10^{-20} cm molecule^{-1} at $T = 296$ K.

In Fig. 7, we illustrate the impact of the MARVELization procedure for the MOTY line list of H_2CS. Here, we compare room temperature spectra of H_2CS computed using the entire

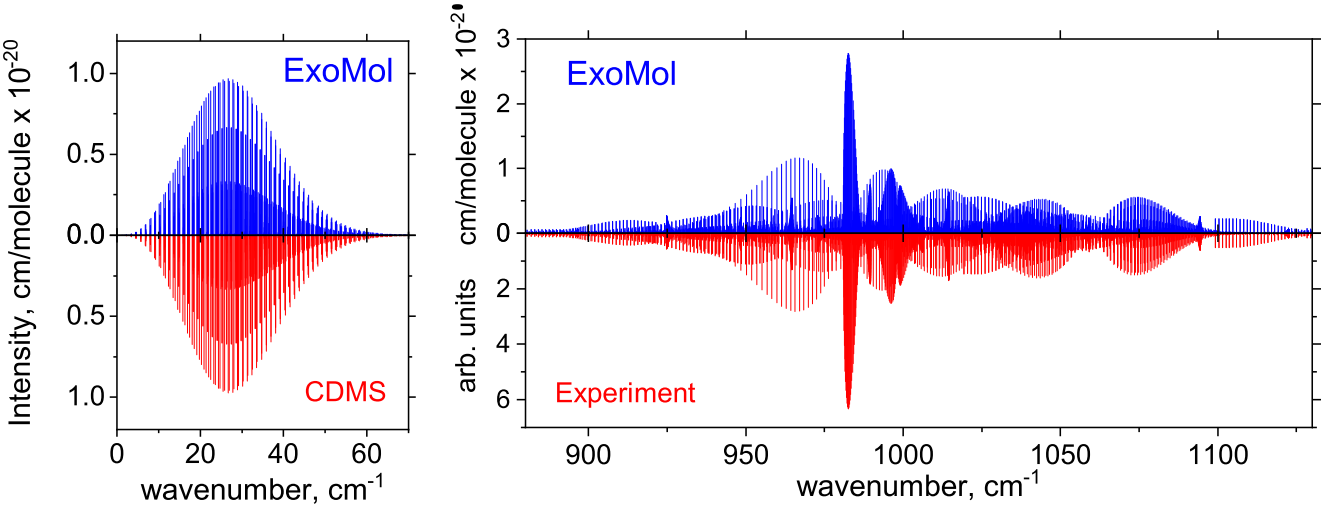

Figure 6. Left: Comparison of ExoMol and CDMS (Endres et al. 2016) microwave absorption cross-sections of H_2CS at $T = 296$ K. Right: Comparison of ExoMol (cm molecule^{-1}) and experimental (arb.units) absorption cross-sections by Flaud et al. (2008) of the $\nu_3/\nu_4/\nu_6$ region of H_2CS at $T = 296$ K.

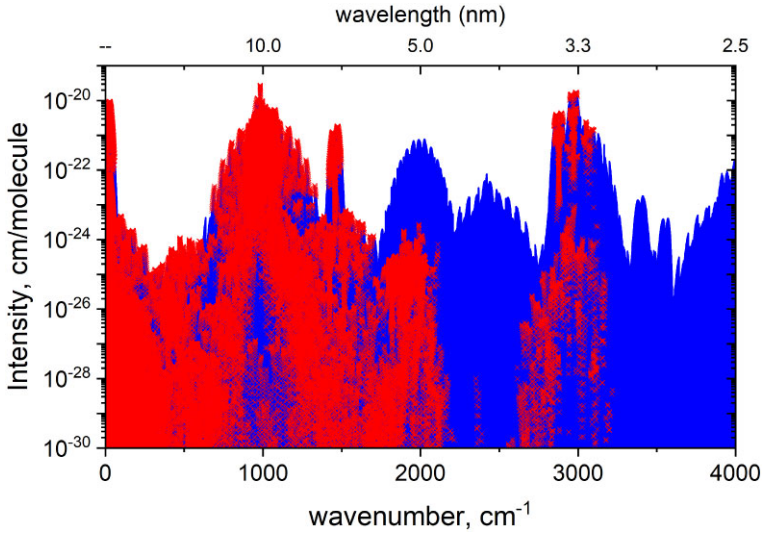

Figure 7. Room temperature ($T = 296$ K) spectra of H_2CS showing the coverage of the MARVELized transitions (red crosses) compared to the total MOTY spectrum.

'unMARVELized' MOTY line list and using the MARVELized (upper and lower) states only. We obtained 81 446 MARVELized transitions of H_2CS with $T = 296$ K intensities below the HITRAN threshold of 10^{-30} /cm^{-1} molecule^{-1}. The total number of H_2CS transitions at $T = 296$ K above this threshold (0–8000 cm^{-1}) is 32 094 935. For example, the weak transitions in the region of 2000 cm^{-1} belong to the hot bands formed from ν_1/ν_5 (upper) and ν_4/ν_6 (lower) states, which have not been experimentally characterized. This figure provides some indication of the H_2CS spectral regions that are suitable for high-resolution applications.

6 CONCLUSION

A hot comprehensive ro–vibrational line list of H_2CS has been presented. The MOTY line list contains over 43.5 billion transitions and covers the 0–8000 cm^{-1} range (wavelengths $\lambda > 1.3$ μm) for states with rotational excitation up to $J = 120$. One of the major improvements over previous H_2CS line lists is the use of a new empirically refined PES. The H_2CS PES is the most accurate to date and was determined by refining to 218 empirically derived MARVEL energy levels up to $J = 5$, leading to orders-of-magnitude improvements in the accuracy of the calculated energy levels, and thus transition wavenumbers. Variational calculations also utilized an exact KEO and a Hamiltonian operator expressed in valence coordinates which greatly improved the convergence of computed energy levels. This enabled a more accurate and extensive line list to be computed as higher J states could be reliably considered. Another significant feature of the MOTY line list is that it has been MARVELized by replacing the calculated energy levels with more accurate empirically derived MARVEL values therefore tailoring the line list to high-resolution applications in certain spectral windows. The prevalence of thioformaldehyde in a variety of astronomical environments means the MOTY line list will be useful for future detection of this molecule. Notably, we expect the MOTY line list to be of relevance to exoplanet atmospheric studies concerned with sulphur chemistry, since H_2CS is a simple organosulphur molecule.

ACKNOWLEDGEMENTS

We thank Andrey Yachmenev for providing us with the potential energy and dipole moment functions of H_2CS. This work was supported by the STFC project nos. ST/M001334/1 and ST/R000476/1. The authors acknowledge the use of the UCL Legion High Performance Computing Facility (Legion@UCL) and associated support services in the completion of this work, along with the Cambridge Service for Data Driven Discovery (CSD3), part of which is operated by the University of Cambridge Research Computing on behalf of the STFC DiRAC HPC Facility (www.dirac.ac.uk). The DiRAC component of CSD3 was funded by BEIS capital funding via STFC capital grant nos. ST/P002307/1 and ST/R002452/1 and STFC operations grant no. ST/R00689X/1. DiRAC is part of the National e-Infrastructure. This work was also supported by the European Research Council (ERC) under the European Union's Horizon 2020 Research and Innovation programme through advance grant no. 883 830.

DATA AVAILABILITY

The data underlying this article are available as part of the supporting information, from the ExoMol data base at www.exomol.com and the CDS data base. The MOTY line list (states, transition, partition function files, and a TROVE input specifying the spectroscopic model of H_2CS) can be downloaded from www.exomol.com[1] and cdsarc.u-strasbg.fr. The open access programmes EXOCROSS and TROVE are available via github.com/exomol.

REFERENCES

Al-Refaie A. F., Yurchenko S. N., Tennyson J., 2017, Comput. Phys. Commun., 214, 216
Bedwell D. J., Duxbury G., 1980, J. Mol. Spectrosc., 84, 531
Beers Y., Klein G. P., Kirchhoff W. H., Johnson D. R., 1972, J. Mol. Spectrosc., 44, 553
Bielska K. et al., 2022, Phys. Rev. Lett., 129, 043002
Birkby J. L., 2018, Handbook of Exoplanets. Cambridge University Press, Cambridge, UK, p. 1485
Bunker P. R., Jensen P., 1998, Molecular Symmetry and Spectroscopy, 2nd edn. NRC Research Press, Ottawa
Clouthier D. J., Huang G., Adam A. G., Merer A. J., 1994, J. Chem. Phys., 101, 7300
Cooley J. W., 1961, Math. Comput., 15, 363
Cox A. P., Hubbard S. D., Kato H., 1982, J. Mol. Spectrosc., 93, 196
Császár A. G., Czakó G., Furtenbacher T., Mátyus E., 2007, Annu. Rep. Comput. Chem., 3, 155
Doddipatla S., He C., Kaiser R. I., Luo Y., Sun R., Galimova G. R., Mebel A. M., Millar T. J., 2020, Proc. Natl. Acad. Sci., 117, 22712
Dunning T. H., Jr, 1989, J. Chem. Phys., 90, 1007
Dunning T. H., Jr, Peterson K. A., Wilson A. K., 2001, J. Chem. Phys., 114, 9244
Endres C. P., Schlemmer S., Schilke P., Stutzki J., Müller H. S. P., 2016, J. Mol. Spectrosc., 327, 95
Erfort S., Tschöpe M., Rauhut G., 2020, J. Chem. Phys., 152, 244104
Esplugues G. et al., 2022, A&A, 662, A52
Fabricant B., Krieger D., Muenter J. S., 1977, J. Chem. Phys., 67, 1576
Flaud J.-M., Lafferty W., Perrin A., Kim Y., Beckers H., Willner H., 2008, J. Quant. Spectrosc. Radiat. Transfer, 109, 995
Furtenbacher T., Császár A. G., 2012, J. Mol. Struct., 1009, 123
Furtenbacher T., Császár A. G., Tennyson J., 2007, J. Mol. Spectrosc., 245, 115
Gardner F. F., Whiteoak J. B., Höglund B., 1980, MNRAS, 191, 19P
He C. et al., 2020, Nat. Astron., 4, 986
Heikkilä A., Johansson L. E. B., Olofsson H., 1999, A&A, 344, 817
Hill C., Yurchenko S. N., Tennyson J., 2013, Icarus, 226, 1673
Hobbs R., Rimmer P. B., Shorttle O., Madhusudhan N., 2021, MNRAS, 506, 3186
Johns J. W. C., Olson W. B., 1971, J. Mol. Spectrosc., 39, 479
Johnson D. R., Powell F. X., 1970, Science, 169, 679
Mcnaughton D., Bruget D. N., 1993, J. Mol. Spectrosc., 159, 340
Maeda A. et al., 2008, ApJS, 176, 543
Martín S., Martín-Pintado J., Mauersberger R., Henkel C., García-Burillo S., 2005, ApJ, 620, 210
Mellor T. M., Owens A., Tennyson J., Yurchenko S. N., 2023, J. Mol. Spectrosc., 391, 111732
Müller H. S. P., Thorwirth S., Roth D. A., Winnewisser G., 2001, A&A, 370, L49
Müller H. S. P., Schlöder F., Stutzki J., Winnewisser G., 2005, J. Mol. Struct., 742, 215
Müller H. S. P. et al., 2019, A&A, 621, A143
Muller S. et al., 2011, A&A, 535, A103
Noumerov B. V., 1924, MNRAS, 84, 592
Sinclair M. W., Fourikis N., Ribes J. C., Robinson B. J., Brown R. D., Godfrey P. D., 1973, Aust. J. Phys., 26, 85
Snellen I., 2014, Phil. Trans. R. Soc. A, 372, 20130075
Sørensen G. O., 1979, Dewar M. J. S. eds, Topics in Current Chemistry, Vol. 82, Large Amplitude Motion in Molecules II. Springer, Berlin, p. 97
Tennyson J., 2014, J. Mol. Spectrosc., 298, 1
Tennyson J., Yurchenko S. N., 2017, Int. J. Quantum Chem., 117, 92
Tennyson J., Hill C., Yurchenko S. N., 2013, AIP Conf. Proc. Vol. 1545, in 6th International Conference on Atomic and Molecular Data and Their Applications ICAMDATA-2012. Am. Inst. Phys., New York, p. 186
Tennyson J. et al., 2020, J. Quant. Spectrosc. Radiat. Transfer, 255, 107228
Tóbiás R., Furtenbacher T., Tennyson J., Császár A. G., 2019, Phys. Chem. Chem. Phys., 21, 3473
Turner P. H., Halonen L., Mills I., 1981, J. Mol. Spectrosc., 88, 402
Woodney L. M., A'Hearn M. F., McMullin J., Samarasinha N., 1997, Earth Moon Planets, 78, 69
Yachmenev A., Yurchenko S. N., 2015, J. Chem. Phys., 143, 014105
Yachmenev A., Yurchenko S. N., Ribeyre T., Thiel W., 2011, J. Chem. Phys., 135, 074302
Yachmenev A., Polyak I., Thiel W., 2013, J. Chem. Phys., 139, 204308
Yurchenko S. N., 2014, in Springborg M., Joswig J.-O., eds, Chemical Modelling: Applications and Theory. The Royal Society of Chemistry, Cambridge, UK, p. 183
Yurchenko S. N., Tennyson J., 2021, in Madhusudhan N., ed., ExoFrontiers: Big questions in exoplanetary science. IOP Publishing, Bristol, p. 21
Yurchenko S. N., Thiel W., Jensen P., 2007, J. Mol. Spectrosc., 245, 126
Yurchenko S. N., Barber R. J., Yachmenev A., Thiel W., Jensen P., Tennyson J., 2009, J. Phys. Chem. A, 113, 11845
Yurchenko S. N., Yachmenev A., Ovsyannikov R. I., 2017, J. Chem. Theory Comput., 13, 4368
Yurchenko S. N., Al-Refaie A. F., Tennyson J., 2018, A&A, 614, A131

SUPPORTING INFORMATION

A *Mathematica* script used to generate the KEO are the refined PES of H_2CS used to compute the line list and the refined PES are provided.

Supplementary data are available at *MNRAS* online.

Please note: Oxford University Press is not responsible for the content or functionality of any supporting materials supplied by the authors. Any queries (other than missing material) should be directed to the corresponding author for the article.

[1] https://exomol.com/data/molecules/H2CS/1H2-12C-32S/MOTY/

APPENDIX: KINETIC ENERGY OPERATOR

We use reduced masses

$$\frac{1}{\mu_{\rm CS}} = \frac{1}{m_{\rm C}} + \frac{1}{m_{\rm S}} \tag{A1}$$

and similarly for the others. Translational components:

$$G_{XX} = G_{YY} = G_{ZZ} = \frac{1}{m_{\rm C} + 2m_{\rm H} + m_{\rm S}}. \tag{A2}$$

Rotational components:

$$\begin{aligned}
G_{XX} &= G_{YY} = \frac{1}{\mu_{\rm CS} r_{\rm CS}^2},\\
G_{XZ} &= \frac{\cot\alpha_{\rm SCH_1}\cos(\tau/2)}{2\mu_{\rm CS} r_{\rm CS}^2} + \frac{\cot\alpha_{\rm SCH_2}\cos(\tau/2)}{2\mu_{\rm CS} r_{\rm CS}^2} - \frac{\csc\alpha_{\rm SCH_1}\cos(\tau/2)}{2m_{\rm C} r_{\rm CS} r_{\rm CH_1}} - \frac{\csc\alpha_{\rm SCH_2}\cos(\tau/2)}{2m_{\rm C} r_{\rm CS} r_{\rm CH_2}},\\
G_{YZ} &= \frac{\cot\alpha_{\rm SCH_2}\sin(\tau/2)}{2\mu_{\rm CS} r_{\rm CS}^2} - \frac{\cot\alpha_{\rm SCH_1}\sin(\tau/2)}{2\mu_{\rm CS} r_{\rm CS}^2} + \frac{\csc\alpha_{\rm SCH_1}\sin(\tau/2)}{2m_{\rm C} r_{\rm CS} r_{\rm CH_1}} - \frac{\csc\alpha_{\rm SCH_2}\sin(\tau/2)}{2m_{\rm C} r_{\rm CS} r_{\rm CH_2}},\\
G_{ZZ} &= \frac{\cot\alpha_{\rm SCH_1}\cot\alpha_{\rm SCH_2}\cos^2(\tau/2)}{2\mu_{\rm CS} r_{\rm CS}^2} - \frac{\cot\alpha_{\rm SCH_1}\cot\alpha_{\rm SCH_2}\sin^2(\tau/2)}{2\mu_{\rm CS} r_{\rm CS}^2} + \frac{\cot^2\alpha_{\rm SCH_1}}{4\mu_{\rm CS} r_{\rm CS}^2}\\
&\quad + \frac{\cot^2\alpha_{\rm SCH_2}}{4\mu_{\rm CS} r_{\rm CS}^2} - \frac{\csc\alpha_{\rm SCH_1}\cot\alpha_{\rm SCH_2}\cos^2(\tau/2)}{2m_{\rm C} r_{\rm CS} r_{\rm CH_1}} + \frac{\csc\alpha_{\rm SCH_1}\cot\alpha_{\rm SCH_2}\sin^2(\tau/2)}{2m_{\rm C} r_{\rm CS} r_{\rm CH_1}}\\
&\quad - \frac{\cot\alpha_{\rm SCH_1}\csc\alpha_{\rm SCH_1}}{2m_{\rm C} r_{\rm CS} r_{\rm CH_1}} - \frac{\cot\alpha_{\rm SCH_1}\csc\alpha_{\rm SCH_2}\cos^2(\tau/2)}{2m_{\rm C} r_{\rm CS} r_{\rm CH_2}} - \frac{\cot\alpha_{\rm SCH_2}\csc\alpha_{\rm SCH_2}}{2m_{\rm C} r_{\rm CS} r_{\rm CH_2}}\\
&\quad + \frac{\cot\alpha_{\rm SCH_1}\csc\alpha_{\rm SCH_2}\sin^2(\tau/2)}{2m_{\rm C} r_{\rm CS} r_{\rm CH_2}} + \frac{\csc^2\alpha_{\rm SCH_1}}{4\mu_{\rm CH} r_{\rm CH_1}^2} + \frac{\csc\alpha_{\rm SCH_1}\csc\alpha_{\rm SCH_2}\cos^2(\tau/2)}{2m_{\rm C} r_{\rm CH_1} r_{\rm CH_2}}\\
&\quad - \frac{\csc\alpha_{\rm SCH_1}\csc\alpha_{\rm SCH_2}\sin^2(\tau/2)}{2m_{\rm C} r_{\rm CH_1} r_{\rm CH_2}} + \frac{\csc^2\alpha_{\rm SCH_2}}{4\mu_{\rm CH} r_{\rm CH_2}^2}.
\end{aligned} \tag{A3}$$

Coriolis components:

$$\begin{aligned}
G_{Xr_{\rm CH_1}} &= \frac{\sin\alpha_{\rm SCH_1}\sin(\tau/2)}{m_{\rm C} r_{\rm CS}},\\
G_{Xr_{\rm CH_2}} &= -\frac{\sin\alpha_{\rm SCH_2}\sin(\tau/2)}{m_{\rm C} r_{\rm CS}},\\
G_{X\alpha_{\rm SCH_1}} &= \frac{\cos\alpha_{\rm SCH_1}\sin(\tau/2)}{m_{\rm C} r_{\rm CS} r_{\rm CH_1}} - \frac{\sin(\tau/2)}{\mu_{\rm CS} r_{\rm CS}^2},\\
G_{X\alpha_{\rm SCH_2}} &= \frac{\sin(\tau/2)}{\mu_{\rm CS} r_{\rm CS}^2} - \frac{\cos\alpha_{\rm SCH_2}\sin(\tau/2)}{m_{\rm C} r_{\rm CS} r_{\rm CH_2}},\\
G_{X\tau} &= \frac{\cot\alpha_{\rm SCH_2}\cos(\tau/2)}{\mu_{\rm CS} r_{\rm CS}^2} + \frac{\csc\alpha_{\rm SCH_1}\cos(\tau/2)}{m_{\rm C} r_{\rm CS} r_{\rm CH_1}} - \frac{\csc\alpha_{\rm SCH_2}\cos(\tau/2)}{m_{\rm C} r_{\rm CS} r_{\rm CH_2}} - \frac{\cot\alpha_{\rm SCH_1}\cos(\tau/2)}{\mu_{\rm CS} r_{\rm CS}^2},\\
G_{Yr_{\rm CH_1}} &= \frac{\sin\alpha_{\rm SCH_1}\cos(\tau/2)}{m_{\rm C} r_{\rm CS}},\\
G_{Yr_{\rm CH_2}} &= \frac{\sin\alpha_{\rm SCH_2}\cos(\tau/2)}{m_{\rm C} r_{\rm CS}},\\
G_{Y\alpha_{\rm SCH_1}} &= \frac{\cos\alpha_{\rm SCH_1}\cos(\tau/2)}{m_{\rm C} r_{\rm CS} r_{\rm CH_1}} - \frac{\cos(\tau/2)}{\mu_{\rm CS} r_{\rm CS}^2},\\
G_{Y\alpha_{\rm SCH_2}} &= \frac{\cos\alpha_{\rm SCH_2}\cos(\tau/2)}{m_{\rm C} r_{\rm CS} r_{\rm CH_2}} - \frac{\cos(\tau/2)}{\mu_{\rm CS} r_{\rm CS}^2},\\
G_{Y\tau} &= \frac{\cot\alpha_{\rm SCH_1}\sin(\tau/2)}{\mu_{\rm CS} r_{\rm CS}^2} + \frac{\cot\alpha_{\rm SCH_2}\sin(\tau/2)}{\mu_{\rm CS} r_{\rm CS}^2} - \frac{\csc\alpha_{\rm SCH_1}\sin(\tau/2)}{m_{\rm C} r_{\rm CS} r_{\rm CH_1}} - \frac{\csc\alpha_{\rm SCH_2}\sin(\tau/2)}{m_{\rm C} r_{\rm CS} r_{\rm CH_2}},\\
G_{Zr_{\rm CH_1}} &= \frac{\sin\alpha_{\rm SCH_1}\cot\alpha_{\rm SCH_2}\sin(\tau/2)\cos(\tau/2)}{m_{\rm C} r_{\rm CS}} - \frac{\sin\alpha_{\rm SCH_1}\csc\alpha_{\rm SCH_2}\sin(\tau/2)\cos(\tau/2)}{m_{\rm C} r_{\rm CH_2}},\\
G_{Zr_{\rm CH_2}} &= \frac{\csc\alpha_{\rm SCH_1}\sin\alpha_{\rm SCH_2}\sin(\tau/2)\cos(\tau/2)}{m_{\rm C} r_{\rm CH_1}} - \frac{\cot\alpha_{\rm SCH_1}\sin\alpha_{\rm SCH_2}\sin(\tau/2)\cos(\tau/2)}{m_{\rm C} r_{\rm CS}},
\end{aligned}$$

$$G_{Z\alpha_{\mathrm{SCH_1}}} = -\frac{\cot\alpha_{\mathrm{SCH_2}}\sin(\tau/2)\cos(\tau/2)}{\mu_{\mathrm{CS}}r_{\mathrm{CS}}^2} + \frac{\cos\alpha_{\mathrm{SCH_1}}\cot\alpha_{\mathrm{SCH_2}}\sin(\tau/2)\cos(\tau/2)}{m_{\mathrm{C}}r_{\mathrm{CS}}r_{\mathrm{CH_1}}} + \frac{\csc\alpha_{\mathrm{SCH_2}}\sin(\tau/2)\cos(\tau/2)}{m_{\mathrm{C}}r_{\mathrm{CS}}r_{\mathrm{CH_2}}} - \frac{\cos\alpha_{\mathrm{SCH_1}}\csc\alpha_{\mathrm{SCH_2}}\sin(\tau/2)\cos(\tau/2)}{m_{\mathrm{C}}r_{\mathrm{CH_1}}r_{\mathrm{CH_2}}},$$

$$G_{Z\alpha_{\mathrm{SCH_2}}} = \frac{\cot\alpha_{\mathrm{SCH_1}}\sin(\tau/2)\cos(\tau/2)}{\mu_{\mathrm{CS}}r_{\mathrm{CS}}^2} - \frac{\csc\alpha_{\mathrm{SCH_1}}\sin(\tau/2)\cos(\tau/2)}{m_{\mathrm{C}}r_{\mathrm{CS}}r_{\mathrm{CH_1}}} - \frac{\cot\alpha_{\mathrm{SCH_1}}\cos\alpha_{\mathrm{SCH_2}}\sin(\tau/2)\csc(\tau/2)}{m_{\mathrm{C}}r_{\mathrm{CS}}r_{\mathrm{CH_2}}} + \frac{\csc\alpha_{\mathrm{SCH_1}}\cos\alpha_{\mathrm{SCH_2}}\sin(\tau/2)\cos(\tau/2)}{m_{\mathrm{C}}r_{\mathrm{CH_1}}r_{\mathrm{CH_2}}},$$

$$G_{Z\tau} = -\frac{\cot^2\alpha_{\mathrm{SCH_1}}}{2\mu_{\mathrm{CS}}r_{\mathrm{CS}}^2} + \frac{\cot^2\alpha_{\mathrm{SCH_2}}}{2\mu_{\mathrm{CS}}r_{\mathrm{CS}}^2} + \frac{\cot\alpha_{\mathrm{SCH_1}}\csc\alpha_{\mathrm{SCH_1}}}{m_{\mathrm{C}}r_{\mathrm{CS}}r_{\mathrm{CH_1}}} - \frac{\cot\alpha_{\mathrm{SCH_2}}\csc\alpha_{\mathrm{SCH_2}}}{m_{\mathrm{C}}r_{\mathrm{CS}}r_{\mathrm{CH_2}}} - \frac{\csc^2\alpha_{\mathrm{SCH_1}}}{2\mu_{\mathrm{CH}}r_{\mathrm{CH_1}}^2} + \frac{\csc^2\alpha_{\mathrm{SCH_2}}}{2\mu_{\mathrm{CH}}r_{\mathrm{CH_2}}^2}.$$

Vibrational components:

$$G_{r_{\mathrm{CS}}r_{\mathrm{CS}}} = \frac{1}{\mu_{\mathrm{CS}}},$$

$$G_{r_{\mathrm{CS}}r_{\mathrm{CH_1}}} = \frac{\cos\alpha_{\mathrm{SCH_1}}}{m_{\mathrm{C}}},$$

$$G_{r_{\mathrm{CS}}r_{\mathrm{CH_2}}} = \frac{\cos\alpha_{\mathrm{SCH_2}}}{m_{\mathrm{C}}},$$

$$G_{r_{\mathrm{CS}}\alpha_{\mathrm{SCH_1}}} = -\frac{\sin\alpha_{\mathrm{SCH_1}}}{m_{\mathrm{C}}r_{\mathrm{CH_1}}},$$

$$G_{r_{\mathrm{CS}}\alpha_{\mathrm{SCH_2}}} = -\frac{\sin\alpha_{\mathrm{SCH_2}}}{m_{\mathrm{C}}r_{\mathrm{CH_2}}},$$

$$G_{r_{\mathrm{CH_1}}r_{\mathrm{CH_1}}} = \frac{1}{\mu_{\mathrm{CH}}},$$

$$G_{r_{\mathrm{CH_1}}r_{\mathrm{CH_2}}} = -\frac{\sin\alpha_{\mathrm{SCH_1}}\sin\alpha_{\mathrm{SCH_2}}\sin^2(\tau/2)}{m_{\mathrm{C}}} + \frac{\sin\alpha_{\mathrm{SCH_1}}\sin\alpha_{\mathrm{SCH_2}}\cos^2(\tau/2)}{m_{\mathrm{C}}} + \frac{\cos\alpha_{\mathrm{SCH_1}}\cos\alpha_{\mathrm{SCH_2}}}{m_{\mathrm{C}}},$$

$$G_{r_{\mathrm{CH_1}}\alpha_{\mathrm{SCH_1}}} = -\frac{\sin\alpha_{\mathrm{SCH_1}}}{m_{\mathrm{C}}r_{\mathrm{CS}}},$$

$$G_{r_{\mathrm{CH_1}}\alpha_{\mathrm{SCH_2}}} = \frac{\sin\alpha_{\mathrm{SCH_1}}\sin^2(\tau/2)}{m_{\mathrm{C}}r_{\mathrm{CS}}} - \frac{\sin\alpha_{\mathrm{SCH_1}}\cos^2(\tau/2)}{m_{\mathrm{C}}r_{\mathrm{CS}}} + \frac{\sin\alpha_{\mathrm{SCH_1}}\cos\alpha_{\mathrm{SCH_2}}\cos^2(\tau/2)}{m_{\mathrm{C}}r_{\mathrm{CH_2}}} - \frac{\sin\alpha_{\mathrm{SCH_1}}\cos\alpha_{\mathrm{SCH_2}}\sin^2(\tau/2)}{m_{\mathrm{C}}r_{\mathrm{CH_2}}} - \frac{\cos\alpha_{\mathrm{SCH_1}}\sin\alpha_{\mathrm{SCH_2}}}{m_{\mathrm{C}}r_{\mathrm{CH_2}}},$$

$$G_{r_{\mathrm{CH_1}}\tau} = \frac{2\sin\alpha_{\mathrm{SCH_1}}\cot\alpha_{\mathrm{SCH_2}}\sin(\tau/2)\cos(\tau/2)}{m_{\mathrm{C}}r_{\mathrm{CS}}} - \frac{2\sin\alpha_{\mathrm{SCH_1}}\csc\alpha_{\mathrm{SCH_2}}\sin(\tau/2)\cos(\tau/2)}{m_{\mathrm{C}}r_{\mathrm{CH_2}}},$$

$$G_{r_{\mathrm{CH_2}}r_{\mathrm{CH_2}}} = \frac{1}{\mu_{\mathrm{CH}}},$$

$$G_{r_{\mathrm{CH_2}}\alpha_{\mathrm{SCH_1}}} = \frac{\sin\alpha_{\mathrm{SCH_2}}\sin^2(\tau/2)}{m_{\mathrm{C}}r_{\mathrm{CS}}} - \frac{\sin\alpha_{\mathrm{SCH_2}}\cos^2(\tau/2)}{m_{\mathrm{C}}r_{\mathrm{CS}}} + \frac{\cos\alpha_{\mathrm{SCH_1}}\sin\alpha_{\mathrm{SCH_2}}\cos^2(\tau/2)}{m_{\mathrm{C}}r_{\mathrm{CH_1}}} - \frac{\cos\alpha_{\mathrm{SCH_1}}\sin\alpha_{\mathrm{SCH_2}}\sin^2(\tau/2)}{m_{\mathrm{C}}r_{\mathrm{CH_1}}} - \frac{\sin\alpha_{\mathrm{SCH_1}}\cos\alpha_{\mathrm{SCH_2}}}{m_{\mathrm{C}}r_{\mathrm{CH_1}}},$$

$$G_{r_{\mathrm{CH_2}}\alpha_{\mathrm{SCH_2}}} = -\frac{\sin\alpha_{\mathrm{SCH_2}}}{m_{\mathrm{C}}r_{\mathrm{CS}}},$$

$$G_{r_{\mathrm{CH_2}}\tau} = \frac{2\cot\alpha_{\mathrm{SCH_1}}\sin\alpha_{\mathrm{SCH_2}}\sin(\tau/2)\cos(\tau/2)}{m_{\mathrm{C}}r_{\mathrm{CS}}} - \frac{2\csc\alpha_{\mathrm{SCH_1}}\sin\alpha_{\mathrm{SCH_2}}\sin(\tau/2)\cos(\tau/2)}{m_{\mathrm{C}}r_{\mathrm{CH_1}}},$$

$$G_{\alpha_{\mathrm{SCH_1}}\alpha_{\mathrm{SCH_1}}} = \frac{1}{\mu_{\mathrm{CS}}r_{\mathrm{CS}}^2} - \frac{2\cos\alpha_{\mathrm{SCH_1}}}{m_{\mathrm{C}}r_{\mathrm{CS}}r_{\mathrm{CH_1}}} + \frac{1}{\mu_{\mathrm{CH}}r_{\mathrm{CH_1}}^2},$$

$$G_{\alpha_{\mathrm{SCH_1}}\alpha_{\mathrm{SCH_2}}} = -\frac{\sin^2(\tau/2)}{\mu_{\mathrm{CS}}r_{\mathrm{CS}}^2} + \frac{\cos^2(\tau/2)}{\mu_{\mathrm{CS}}r_{\mathrm{CS}}^2} - \frac{\cos\alpha_{\mathrm{SCH_1}}\cos^2(\tau/2)}{m_{\mathrm{C}}r_{\mathrm{CS}}r_{\mathrm{CH_1}}} + \frac{\cos\alpha_{\mathrm{SCH_1}}\sin^2(\tau/2)}{m_{\mathrm{C}}r_{\mathrm{CS}}r_{\mathrm{CH_1}}} - \frac{\cos\alpha_{\mathrm{SCH_2}}\cos^2(\tau/2)}{m_{\mathrm{C}}r_{\mathrm{CS}}r_{\mathrm{CH_2}}} + \frac{\cos\alpha_{\mathrm{SCH_2}}\sin^2(\tau/2)}{m_{\mathrm{C}}r_{\mathrm{CS}}r_{\mathrm{CH_2}}} + \frac{\sin\alpha_{\mathrm{SCH_1}}\sin\alpha_{\mathrm{SCH_2}}}{m_{\mathrm{C}}r_{\mathrm{CH_1}}r_{\mathrm{CH_2}}} - \frac{\cos\alpha_{\mathrm{SCH_1}}\cos\alpha_{\mathrm{SCH_2}}\sin^2(\tau/2)}{m_{\mathrm{C}}r_{\mathrm{CH_1}}r_{\mathrm{CH_2}}} + \frac{\cos\alpha_{\mathrm{SCH_1}}\cos\alpha_{\mathrm{SCH_2}}\cos^2(\tau/2)}{m_{\mathrm{C}}r_{\mathrm{CH_1}}r_{\mathrm{CH_2}}}.$$

$$
\begin{aligned}
G_{\alpha_{\mathrm{SCH}_1}\tau} &= -\frac{2\cot\alpha_{\mathrm{SCH}_2}\sin(\tau/2)\cos(\tau/2)}{\mu_{\mathrm{CS}}r_{\mathrm{CS}}^2} + \frac{2\cos\alpha_{\mathrm{SCH}_1}\cot\alpha_{\mathrm{SCH}_2}\sin(\tau/2)\cos(\tau/2)}{m_{\mathrm{C}}r_{\mathrm{CS}}r_{\mathrm{CH}_1}} \\
&\quad + \frac{2\csc\alpha_{\mathrm{SCH}_2}\sin(\tau/2)\cos(\tau/2)}{m_{\mathrm{C}}r_{\mathrm{CS}}r_{\mathrm{CH}_2}} - \frac{2\cos\alpha_{\mathrm{SCH}_1}\csc\alpha_{\mathrm{SCH}_2}\sin(\tau/2)\cos(\tau/2)}{m_{\mathrm{C}}r_{\mathrm{CH}_1}r_{\mathrm{CH}_2}}, \\
G_{\alpha_{\mathrm{SCH}_2}\alpha_{\mathrm{SCH}_2}} &= \frac{1}{\mu_{\mathrm{CS}}r_{\mathrm{CS}}^2} - \frac{2\cos\alpha_{\mathrm{SCH}_2}}{m_{\mathrm{C}}r_{\mathrm{CS}}r_{\mathrm{CH}_2}} + \frac{1}{\mu_{\mathrm{CH}}r_{\mathrm{CH}_2}^2}, \\
G_{\alpha_{\mathrm{SCH}_2}\tau} &= -\frac{2\cot\alpha_{\mathrm{SCH}_1}\sin(\tau/2)\cos(\tau/2)}{\mu_{\mathrm{CS}}r_{\mathrm{CS}}^2} + \frac{2\cot\alpha_{\mathrm{SCH}_1}\cos\alpha_{\mathrm{SCH}_2}\sin(\tau/2)\cos(\tau/2)}{m_{\mathrm{C}}r_{\mathrm{CS}}r_{\mathrm{CH}_2}} \\
&\quad - \frac{2\csc\alpha_{\mathrm{SCH}_1}\cos\alpha_{\mathrm{SCH}_2}\sin(\tau/2)\cos(\tau/2)}{m_{\mathrm{C}}r_{\mathrm{CH}_1}r_{\mathrm{CH}_2}} + \frac{2\csc\alpha_{\mathrm{SCH}_1}\sin(\tau/2)\cos(\tau/2)}{m_{\mathrm{C}}r_{\mathrm{CS}}r_{\mathrm{CH}_1}}, \\
G_{\tau\tau} &= -\frac{2\cot\alpha_{\mathrm{SCH}_1}\cot\alpha_{\mathrm{SCH}_2}\cos^2(\tau/2)}{\mu_{\mathrm{CS}}r_{\mathrm{CS}}^2} + \frac{2\cot\alpha_{\mathrm{SCH}_1}\cot\alpha_{\mathrm{SCH}_2}\sin^2(\tau/2)}{m_{\mathrm{C}}r_{\mathrm{CS}}^2} + \frac{\cot^2\alpha_{\mathrm{SCH}_1}}{\mu_{\mathrm{CS}}r_{\mathrm{CS}}^2} \\
&\quad + \frac{\cot^2\alpha_{\mathrm{SCH}_2}}{\mu_{\mathrm{CS}}r_{\mathrm{CS}}^2} + \frac{2\csc\alpha_{\mathrm{SCH}_1}\cot\alpha_{\mathrm{SCH}_2}\cos^2(\tau/2)}{m_{\mathrm{C}}r_{\mathrm{CS}}r_{\mathrm{CH}_1}} - \frac{2\csc\alpha_{\mathrm{SCH}_1}\cot\alpha_{\mathrm{SCH}_2}\sin^2(\tau/2)}{m_{\mathrm{C}}r_{\mathrm{CS}}r_{\mathrm{CH}_1}} \\
&\quad - \frac{2\cot\alpha_{\mathrm{SCH}_1}\csc\alpha_{\mathrm{SCH}_1}}{m_{\mathrm{C}}r_{\mathrm{CS}}r_{\mathrm{CH}_1}} + \frac{2\cot\alpha_{\mathrm{SCH}_1}\csc\alpha_{\mathrm{SCH}_2}\cos^2(\tau/2)}{m_{\mathrm{C}}r_{\mathrm{CS}}r_{\mathrm{CH}_2}} + \frac{\csc^2\alpha_{\mathrm{SCH}_1}}{\mu_{\mathrm{CH}}r_{\mathrm{CH}_1}^2} \\
&\quad - \frac{2\cot\alpha_{\mathrm{SCH}_1}\csc\alpha_{\mathrm{SCH}_2}\sin^2(\tau/2)}{\mu_{\mathrm{CS}}r_{\mathrm{CS}}r_{\mathrm{CH}_2}} - \frac{2\cot\alpha_{\mathrm{SCH}_2}\csc\alpha_{\mathrm{SCH}_2}}{m_{\mathrm{C}}r_{\mathrm{CS}}r_{\mathrm{CH}_2}} + \frac{\csc^2\alpha_{\mathrm{SCH}_2}}{\mu_{\mathrm{CH}}r_{\mathrm{CH}_2}^2} \\
&\quad - \frac{2\csc\alpha_{\mathrm{SCH}_1}\csc\alpha_{\mathrm{SCH}_2}\cos^2(\tau/2)}{m_{\mathrm{C}}r_{\mathrm{CH}_1}r_{\mathrm{CH}_2}} + \frac{2\csc\alpha_{\mathrm{SCH}_1}\csc\alpha_{\mathrm{SCH}_2}\sin^2(\tau/2)}{m_{\mathrm{C}}r_{\mathrm{CH}_1}r_{\mathrm{CH}_2}}.
\end{aligned}
$$

Pseudo-potential:

$$
\begin{aligned}
U = &-\frac{\cot\alpha_{\mathrm{SCH}_1}\cot\alpha_{\mathrm{SCH}_2}\cos^2(\tau/2)}{4\mu_{\mathrm{CS}}r_{\mathrm{CS}}^2} + \frac{\cot\alpha_{\mathrm{SCH}_2}\csc\alpha_{\mathrm{SCH}_1}\cos^2(\tau/2)}{4m_{\mathrm{C}}r_{\mathrm{CS}}r_{\mathrm{CH}_1}} + \frac{\cot\alpha_{\mathrm{SCH}_1}\csc\alpha_{\mathrm{SCH}_2}\cos^2(\tau/2)}{4m_{\mathrm{C}}r_{\mathrm{CS}}r_{\mathrm{CH}_2}} \\
&- \frac{\csc\alpha_{\mathrm{SCH}_1}\csc\alpha_{\mathrm{SCH}_2}\cos^2(\tau/2)}{4m_{\mathrm{C}}r_{\mathrm{CH}_1}r_{\mathrm{CH}_2}} + \frac{\cot\alpha_{\mathrm{SCH}_2}\sin\alpha_{\mathrm{SCH}_1}\cos^2(\tau/2)}{4m_{\mathrm{C}}r_{\mathrm{CS}}r_{\mathrm{CH}_1}} - \frac{\csc\alpha_{\mathrm{SCH}_2}\sin\alpha_{\mathrm{SCH}_1}\cos^2(\tau/2)}{4m_{\mathrm{C}}r_{\mathrm{CH}_1}r_{\mathrm{CH}_2}} \\
&+ \frac{\cot\alpha_{\mathrm{SCH}_1}\sin\alpha_{\mathrm{SCH}_2}\cos^2(\tau/2)}{4m_{\mathrm{C}}r_{\mathrm{CS}}r_{\mathrm{CH}_2}} - \frac{\csc\alpha_{\mathrm{SCH}_1}\sin\alpha_{\mathrm{SCH}_2}\cos^2(\tau/2)}{4m_{\mathrm{C}}r_{\mathrm{CH}_1}r_{\mathrm{CH}_2}} - \frac{\sin\alpha_{\mathrm{SCH}_1}\sin\alpha_{\mathrm{SCH}_2}\cos^2(\tau/2)}{4m_{\mathrm{C}}r_{\mathrm{CH}_1}r_{\mathrm{CH}_2}} \\
&+ \frac{\cot^2\alpha_{\mathrm{SCH}_1}}{32\mu_{\mathrm{CS}}r_{\mathrm{CS}}^2} - \frac{\cot^2\alpha_{\mathrm{SCH}_1}}{16\mu_{\mathrm{CH}}r_{\mathrm{CH}_1}^2} + \frac{\cot^2\alpha_{\mathrm{SCH}_2}}{32\mu_{\mathrm{CS}}r_{\mathrm{CS}}^2} - \frac{\cot^2\alpha_{\mathrm{SCH}_2}}{16\mu_{\mathrm{CH}}r_{\mathrm{CH}_2}^2} - \frac{5\csc^2\alpha_{\mathrm{SCH}_1}}{32\mu_{\mathrm{CS}}r_{\mathrm{CS}}^2} - \frac{\csc^2\alpha_{\mathrm{SCH}_1}}{16\mu_{\mathrm{CH}}r_{\mathrm{CH}_1}^2} - \frac{5\csc^2\alpha_{\mathrm{SCH}_2}}{32\mu_{\mathrm{CS}}r_{\mathrm{CS}}^2} \\
&- \frac{\csc^2\alpha_{\mathrm{SCH}_2}}{16\mu_{\mathrm{CH}}r_{\mathrm{CH}_2}^2} + \frac{\cot\alpha_{\mathrm{SCH}_1}\cot\alpha_{\mathrm{SCH}_2}\sin^2(\tau/2)}{4\mu_{\mathrm{CS}}r_{\mathrm{CS}}^2} - \frac{\cot\alpha_{\mathrm{SCH}_2}\csc\alpha_{\mathrm{SCH}_1}\sin^2(\tau/2)}{4m_{\mathrm{C}}r_{\mathrm{CS}}r_{\mathrm{CH}_1}} \\
&- \frac{\cot\alpha_{\mathrm{SCH}_1}\csc\alpha_{\mathrm{SCH}_2}\sin^2(\tau/2)}{4m_{\mathrm{C}}r_{\mathrm{CS}}r_{\mathrm{CH}_2}} + \frac{\csc\alpha_{\mathrm{SCH}_1}\csc\alpha_{\mathrm{SCH}_2}\sin^2(\tau/2)}{4m_{\mathrm{C}}r_{\mathrm{CH}_1}r_{\mathrm{CH}_2}} - \frac{\cot\alpha_{\mathrm{SCH}_2}\sin\alpha_{\mathrm{SCH}_1}\sin^2(\tau/2)}{4m_{\mathrm{C}}r_{\mathrm{CS}}r_{\mathrm{CH}_1}} \\
&+ \frac{\csc\alpha_{\mathrm{SCH}_2}\sin\alpha_{\mathrm{SCH}_1}\sin^2(\tau/2)}{4m_{\mathrm{C}}r_{\mathrm{CH}_1}r_{\mathrm{CH}_2}} - \frac{\cot\alpha_{\mathrm{SCH}_1}\sin\alpha_{\mathrm{SCH}_2}\sin^2(\tau/2)}{4m_{\mathrm{C}}r_{\mathrm{CS}}r_{\mathrm{CH}_2}} + \frac{\csc\alpha_{\mathrm{SCH}_1}\sin\alpha_{\mathrm{SCH}_2}\sin^2(\tau/2)}{4m_{\mathrm{C}}r_{\mathrm{CH}_1}r_{\mathrm{CH}_2}} \\
&+ \frac{\sin\alpha_{\mathrm{SCH}_1}\sin\alpha_{\mathrm{SCH}_2}\sin^2(\tau/2)}{4m_{\mathrm{C}}r_{\mathrm{CH}_1}r_{\mathrm{CH}_2}} - \frac{\cos\alpha_{\mathrm{SCH}_1}}{4m_{\mathrm{C}}r_{\mathrm{CS}}r_{\mathrm{CH}_1}} - \frac{\cos\alpha_{\mathrm{SCH}_1}\cos\alpha_{\mathrm{SCH}_2}}{4m_{\mathrm{C}}r_{\mathrm{CH}_1}r_{\mathrm{CH}_2}} - \frac{\cos\alpha_{\mathrm{SCH}_2}}{4m_{\mathrm{C}}r_{\mathrm{CS}}r_{\mathrm{CH}_2}} \\
&+ \frac{\cot\alpha_{\mathrm{SCH}_1}\csc\alpha_{\mathrm{SCH}_1}}{4m_{\mathrm{C}}r_{\mathrm{CS}}r_{\mathrm{CH}_1}} + \frac{\cot\alpha_{\mathrm{SCH}_2}\csc\alpha_{\mathrm{SCH}_2}}{4m_{\mathrm{C}}r_{\mathrm{CS}}r_{\mathrm{CH}_2}} - \frac{3}{16\mu_{\mathrm{CS}}r_{\mathrm{CS}}^2} - \frac{3}{16\mu_{\mathrm{CS}}r_{\mathrm{CH}_1}^2} - \frac{3}{16\mu_{\mathrm{CH}}r_{\mathrm{CH}_2}^2}.
\end{aligned}
$$

This paper has been typeset from a TEX/LATEX file prepared by the author.